Steady-state helices of the actin homolog MreB inside bacteria: Dynamics without motors

Jun F. Allard and Andrew D. Rutenberg*
Department of Physics and Atmospheric Science, Dalhousie University, Halifax, Nova Scotia, Canada B3H 3J5
(Received 21 March 2007; published 14 September 2007)

Within individual bacteria, we combine force-dependent polymerization dynamics of individual MreB protofilaments with an elastic model of protofilament bundles buckled into helical configurations. We use variational techniques and stochastic simulations to relate the pitch of the MreB helix, the total abundance of MreB, and the number of protofilaments. By comparing our simulations with mean-field calculations, we find that stochastic fluctuations are significant. We examine the quasistatic evolution of the helical pitch with cell growth, as well as time scales of helix turnover and *de novo* establishment. We find that while the body of a polarized MreB helix treadmills toward its slow-growing end, the fast-growing tips of laterally associated protofilaments move toward the opposite fast-growing end of the MreB helix. This offers a possible mechanism for targeted polar localization without cytoplasmic motor proteins.

DOI: 10.1103/PhysRevE.76.031916 PACS number(s): 87.16.Ka, 87.16.Ac, 87.15.La, 87.15.Rn

I. INTRODUCTION

The eukaryotic cytoskeleton organizes cell shape, cell polarity, cell division, and nondiffusive subcellular transport. F-actin, microtubules, and intermediate filaments comprise the cytoskeleton and act with associated proteins, which provides spatial and dynamic control of the cytoskeletal function [1]. Prokaryotic cells have cytoskeletal analogs, such as the FtsZ ring associated with cell division [2] together with its "divisome" of associated proteins. Bacteria also have a number of polymerizing cytoplasmic proteins, such as ParM [3] and MinD [2], that exhibit distinctive helical structures within the cell.

Recently, the actin homolog MreB has been shown to play a cytoskeletal role in many bacteria [2,4,5]. MreB forms a continuous cytoplasmic helix that runs the length of nearly all rod-shaped prokaryotes, including *Escherichia coli*, *Bacillus subtilis*, and *Caulobacter crescentus* [6], and it has been implicated in shape determination and polar protein localization.

In most Gram-positive bacteria MreB is present together with several paralogues, such as Mbl and MreBH in *B. subtilis*. The helical pitches for MreB or Mbl, separately observed by immunoflourescence microscopy, are reported to be 0.73 ± 0.12 μm and 1.7 ± 0.28 μm, respectively [7]. More recent measurements of fluorescent fusions of MreB and of Mbl report pitches of 0.6 ± 0.14 μm, with colocalization [8]. In Gram-negative species, such as *E. coli* and *C. crescentus*, only MreB is present. In *E. coli*, pitches of 0.46 ± 0.08 μm have been reported [9]. In all cases, the helices are dynamic, with elements moving along the main helix at reported speeds ranging from 6 nm/s [10] to 70 nm/s [11]. The helical structure has also been observed to condense into a ring at midcell near the time of division in *E. coli* [12], *C. crescentus* [13], and *B. subtilis* (where only MreBH coils) [14].

The MreB helix appears to be composed of a bundle of individual "protofilaments" [15–17]. Quantitative immunoblotting has been used to measure the molecular abundance of various MreBs. In *B. subtilis*, there are roughly 8000 MreB monomers and 12 000–14 000 monomers of Mbl [7] while *E. coli* has roughly 17 000–40 000 monomers of MreB [9]. Neglecting the cytoplasmic fraction of monomeric MreB, these abundances suggest a bundle thickness of about 10 protofilaments [18].

In *B. subtilis*, Mbl is necessary for proper insertion of new peptidoglycan, which occurs in a helical fashion [6], while MreBH is necessary for the localization and function of the cell wall hydrolase LytE, which is believed to recycle the outer layers of the cell wall, also in a helical fashion [14]. Cells with mutant *mreB* are wide, rounded, and usually not viable [19]. Helical bundles of MreB may contribute to the spatial localization of associated MreC, MreD, and PBP2, which, in turn, help to coordinate cell wall synthesis. It has also been suggested that helical filaments of MreB paralogues under tension can lead to spiral morphologies [20].

Disruption of MreB leads to loss of proper polar localization of a number of proteins such as the chemotaxis protein Tar and the *Shigella flexneri* virulence factor IcsA in *E. coli* [21] and three integral membrane proteins (PleC, DivJ, CckA) in *C. crescentus* [22]. Polar localization in *C. crescentus* was disrupted by either underexpression or overexpression of MreB. When normal MreB expression was returned, polar localization was reestablished [22]. This suggests that MreB has a continual role in either direct polar trafficking of these proteins or in the maintenance of landmarks necessary for their proper positioning [4].

The polar proteins in *C. crescentus* are normally directed toward distinct (stalked and swarmer) poles in different stages (swarmer, stalked, and predivisional) of its life cycle. For example, PleC is localized to swarmer poles in swarmer and predivisional cells and DivJ is localized to stalked poles, while CckA is localized to both poles of predivisional cells [23]. After MreB expression is disrupted and restored, PleC and DivJ are restored *randomly* to either pole [23]. This suggests that MreB may be polarized within *C. crescentus* and that the polarity of the MreB helix is randomly restored after its disruption. However, tracking of individual YFP-MreB molecules shows unpolarized motion [10], raising questions about the mechanism of specific polar targeting. MreB-directed targeting to specific poles has not been reported in

*andrew.rutenberg@dal.ca

E. coli or *B. subtilis*.

MreB interacts with both RNA polymerase (RNAP) [23] and SetB, a chromosome defect suppressor [24], and has been implicated in the fast polar translocation of the origin-proximal regions (*oriC*) [27] of newly-replicated DNA in *C. crescentus* [25] and in *E. coli* [23] (see, however, [26]). Time-lapse microscopy has shown that the polar transport of *oriC* in *B. subtilis* had an average speed of 2.8 nm/s and a peak speed of 4.5 nm/s [27].

MreB is a homolog of the eukaryotic cytoskeletal protein actin [28,29]. Actin filaments are used to change cell shape and to move bacteria such as *Listeria monocytogenes* via polymerization forces [30] and in muscle contraction and for organelle movement via collections of myosin motor proteins [1]. Actin assembly is regulated through a number of "actin-binding proteins" that variously control cross-linking, bundling, filament nucleation, end-capping, filament cutting, monomer sequestration, and desequestration. MreB, in contrast, does not have any clearly identified motor proteins or associated proteins that regulate polymerization. Notably, MreB filaments spontaneously bundle *in vitro* without associated proteins [31].

The varied roles of MreB inside bacterial cells raise some basic questions. What is the origin of its helical configuration, and how significant are the forces that the MreB helix applies? What does the helical pitch of MreB filaments depend on? What aspects of the MreB system can be understood in terms of actin-like polymerization dynamics? Specifically, must we invoke yet-to-be-discovered prokaryotic motor proteins or accessory proteins controlling MreB polymerization to explain MreB-related polar localization of proteins such as Tar, IcsA, DivJ, PleC, and CckA? Finally, does the small size of the bacterial cell affect MreB polymerization, as compared to actin polymerization in much larger eukaryotic cells?

To address these questions, we present a model of the MreB helix with stochastic polymerization dynamics of protofilaments together with global elasticity of a helical MreB bundle constrained by the bacterial cell wall. Our model provides a quantitative relationship between helical pitch, total abundance of MreB protein in a particular cell, and the thickness of the protofilament bundles. The bundled MreB protofilaments are in a dynamical steady-state and undergo constant advection as the polymerized subunits treadmill. We discuss how this advection could be harnessed for targeted polar localization without motor proteins. The steady-state dynamics also allows us to address other dynamical processes such as protein turnover in FRAP experiments [32] or recovery from A22-induced disruptions of the MreB helix [22].

II. MODEL

A. Protofilament polymerization

Both actin and MreB polymerize into polarized filaments. Addition and dissociation of monomers occur at the ends of the asymmetric filament, at both the "barbed" ("+" or fast-growing) tip and the "pointed" ("–" or slow-growing) tip. The kinetics of actin polymerization is well characterized by concentration-dependent polymerization rates $k^b_{\rm on}c$ and $k^p_{\rm on}c$ at the barbed and pointed ends, respectively, where c is the cytoplasmic monomer concentration, and concentration-independent depolymerization rates $k^b_{\rm off}$ and $k^p_{\rm off}$.

If a force F is applied to a filament's tip, the polymerization rate is reduced. When thermal bending fluctuations are much faster than the polymerization dynamics, the polymerization rates at either end of the filament are reduced to [30]

$$k_{\rm on}ce^{-Fa_0/k_BT}, \tag{1}$$

where a_0=5.1 nm is the MreB monomer length [33] and k_BT=4.1 pN nm at room temperature. This force-dependent polymerization rate can also be obtained from thermodynamic arguments in the high-force limit [34]. We apply it to MreB polymerization dynamics within the cell.

In the absence of force, each filament grows above, and shrinks below, the critical cytoplasmic concentration

$$c_c = \frac{k^b_{\rm off} + k^p_{\rm off}}{k^b_{\rm on} + k^p_{\rm on}}. \tag{2}$$

The asymmetry between the polymerization and depolymerization rates at barbed and pointed ends leads to treadmilling, in which the filament length remains constant while depolymerization from the pointed end is balanced by polymerization at the barbed end [1]. The force-independent treadmilling rate is [35]

$$\lambda_{tread} = \frac{k^p_{\rm off}k^b_{\rm on} - k^b_{\rm off}k^p_{\rm on}}{k^p_{\rm on} + k^b_{\rm on}}. \tag{3}$$

If the filament position is fixed, treadmilling results in a net advection of all polymerized monomers toward the pointed end.

The kinetic rate constants for MreB polymerization are yet to be determined explicitly, but appear to differ significantly from eukaryotic actin. In addition to spontaneously nucleating and bundling with much greater ease than actin, purified MreB from *Thermotoga maritima* polymerizes *in vitro* faster and exhibits a much lower critical concentration ($c_{c,\rm MreB}$=0.003 μM [31] compared with $c_{c,\rm actin}$=0.17 μM [10]). Nevertheless, *in vivo* observations of single-molecule motion of MreB in *C. crescentus* suggest that the treadmilling rate is similar to actin [10]. By starting with *in vitro* rate constants from eukaryotic actin [29] and scaling the on-rates by a factor of $c_{c,\rm actin}/c_{c,\rm MreB}$=55, we recover the reported critical concentration of *in vitro* MreB from *T. maritima*. Following *in vitro* observations that the treadmilling rate is $\lambda_{\rm MreB}$=1.2 s^{-1} [10], we further scale all four rates by $\lambda_{\rm MreB}/\lambda_{\rm actin}$=2.1—preserving the MreB treadmilling rate. These scalings preserve the pointed- and barbed-end asymmetries of actin and represent the least-intrusive modification of actin polymerization dynamics to make it consistent with the observed MreB dynamics. The resulting barbed-end polymerization rate constant k^b_{on} (see Table I) is close to the diffusion limit [36] indicating that the pointed- and barbed-end asymmetries of MreB may differ significantly from actin and/or that the appropriate c_c for *in vivo* measurements may be significantly above the *T. maritima* value. However, our

TABLE I. The parameters used in this paper for MreB and its paralogues. Only c_c and a_0 have been directly measured for MreB from *T. maritima*. Other assumed parameters have been extracted from the properties of eukaryotic actin, which is homologous. The kinetic rates chosen for MreB recover c_c [31] and the *in vivo* treadmilling rate [10], but leave the pointed and barbed asymmetry unchanged. The elastic moduli are for a single protofilament of F-actin ($n=1$).

Symbol	Value	Meaning	Reference
Eukaryotic actin kinetic rates for polymerization			
k_{on}^{b}	12 $\mu\mathrm{M}^{-1}\ \mathrm{s}^{-1}$	Barbed-end addition rate constant	[29]
k_{on}^{p}	1.3 $\mu\mathrm{M}^{-1}\ \mathrm{s}^{-1}$	Pointed-end addition rate constant	[29]
k_{off}^{b}	1.4 s^{-1}	Barbed-end dissociation rate	[29]
k_{off}^{p}	0.8 s^{-1}	Pointed-end dissociation rate	[29]
c_c	0.167 $\mu\mathrm{M}$	Critical concentration	[Eq. (2) and [29]]
λ_{tread}	0.58 s^{-1}	Free treadmilling rate	[Eq. (3) and [29]]
Assumed MreB kinetic rates for polymerization			
k_{on}^{b}	1360 $\mu\mathrm{M}^{-1}\ \mathrm{s}^{-1}$	Barbed-end addition rate constant	(scaled to fit c_c and λ)
k_{on}^{p}	150 $\mu\mathrm{M}^{-1}\ \mathrm{s}^{-1}$	Pointed-end addition rate constant	(scaled to fit c_c and λ)
k_{off}^{b}	2.9 s^{-1}	Barbed-end dissociation rate	(scaled to fit c_c and λ)
k_{off}^{p}	1.7 s^{-1}	Pointed-end dissociation rate	(scaled to fit c_c and λ)
c_c	0.003 $\mu\mathrm{M}$	Critical concentration	[31]
λ_{tread}	1.2 s^{-1}	Free treadmilling rate	[10]
B	1.0×10^{4} pN nm^2	Bending modulus of MreB protofilament	(from actin [60])
E	20 pN	Stretching modulus of MreB protofilament	(from actin [60])
a_0	5.1 nm	Monomer spacing of MreB	[31]
R_c	400 nm	Radius of *B. subtilis* cell	[14]
L_c	$(2-4)\times10^{3}$ nm	Length of cylindrical portion of *B. subtilis* cell	[14]
η	10^{-9} pN $\mathrm{s/nm}^2$	Cytoplasmic viscosity	[61]

qualitative results do not depend on the precise parameter values used in this paper.

We model polymerization dynamics by the stochastic addition and dissociation of monomers at the barbed and pointed ends of individual MreB protofilaments [17] using the scaled kinetic rate constants discussed above and listed, together with other parameters, in Table I. Except for growing cells in Sec. III B, a standard cell length of $L_c=3$ μm and cell radius of $R_c=400$ nm are used.

B. Bundle ultrastructure

The ultrastructure of the MreB helix—the precise arrangement, orientation, and length distribution of the individual protofilaments that make up the helical bundle—remains a mystery. Several hypotheses have been put forward [16], and Fig. 1 illustrates five basic possibilities. Several of these are less plausible. The slippery arrays in Fig. 1(e) are unlikely to be able to support the forces the cytoskeleton must withstand as it pushes against the cell wall, and recent biochemical experiments have demonstrated large lateral interactions between filaments [31]. The ultrastructure in Fig. 1(c) leads to tapered bundles as antiparallel protofilaments, which cannot slide past each other, treadmill in opposite directions. Such tapering is not seen experimentally. In this paper we therefore consider ultrastructures composed of polarized bundle(s) of protofilaments: either one bundle [Fig. 1(a)] or two antiparallel bundles that freely slide with respect to each other [Fig. 1(d)]. Since the elastic and polymerization properties of the second case follow straightforwardly from the former, we will mostly focus on a single polarized nonslipping filament bundle [Fig. 1(a)] and reexamine the possibility of antiparallel bundles slipping with respect to each other in the final discussion.

It is quite possible that individual MreB protofilaments do not continuously extend from one end of the bacterial cell to the other, similar to actin cables in yeast [37]. Indeed, in *C. crescentus* individual protofilaments appear to be much shorter than the cell length, only 392 ± 23 nm on average [10]. For the purposes of our model, the mechanical and end-polymerization properties of discontinuous bundles of protofilaments are equivalent to bundles of continuous protofilaments. Systematic heterogeneities in the MreB helix thickness have not been reported, but our model does not depend on how the cell regulates the average number of protofilaments in a cross section of the filament bundle. Protofilament association, dissociation, and nucleation are thus implicitly included in our model. Polymerization and depolymerization away from the filament edges may occur and do not affect our steady-state results: whatever the distribution of lateral exchange, in a steady state, monomer incorporation and separation are balanced. Of course, significant numbers of active protofilament tips away from the cell poles can affect the dynamical time scales that we discuss.

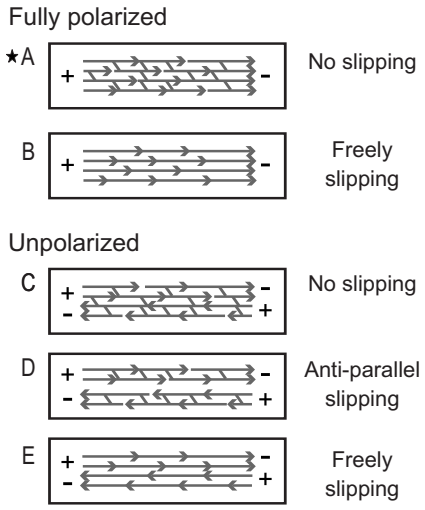

FIG. 1. Five models for the MreB ultrastructure, each composed of polarized protofilaments. (a) Single polarized bundle of protofilaments with lateral interactions that prevent relative slipping within the bundle. As indicated by the star, data in subsequent figures are for this model. (b) Polarized bundle of protofilaments that freely slip relative to each other. (c) Unpolarized bundle of protofilaments, with no lateral slipping. (d) Two antiparallel bundles of polarized protofilaments that slip relative to each other, though protofilaments within a given bundle do not slip. (e) Unpolarized bundle of protofilaments that all freely slip with respect to each other.

C. Elastic bundle

In vitro, MreB typically polymerizes into straight filaments [2]. However, MreB adopts ringlike coiled configurations in spherical mutants of normally rod-shaped organisms [38] and forms helices in rod-shaped cells [15]. These observations suggest that normally straight elastic MreB protofilaments may simply buckle into helices inside the cylindrical confinement provided by the relatively hard cell wall.

A self-consistent model for the observed MreB helices consists of a particular ultrastructure of protofilaments, as in Fig. 1, buckled into a helical configuration by the cylindrical cell wall. A steady state exists where the polymerization force at the tips of the helices is balanced by the mechanical forces of the helical configuration. We treat the cell as a spherocylinder with total length L_c+2R_c and radius R_c and total volume $\pi R_c^2(L_c+2R_c)$. The helix is assumed to extend throughout the cylindrical part of the cell, but not into the hemispherical poles, as indicated by experiment [7].

Although helical equilibria of elastic filaments have been investigated since the 1800s, they remain a contemporary topic [39]. In the elastic Cosserat model [40], a filament is parametrized by its unstretched arclength $s \in [0, L_{fil}]$ where L_{fil} is its total unstretched length. The elastic energy of such a filament is

$$\mathcal{H} = \frac{1}{2}\int_0^{L_{fil}} \{[B\kappa(s)^2 + C\tau(s)^2]n(s)^2 + E(1-|\partial\vec{r}/\partial s|)^2 n(s)\} ds, \tag{4}$$

where $\vec{r}(s)$ is the position of the centerline, $\kappa(s)$ is the local curvature, $\tau(s)$ is the local twist, and $n(s)$ is the local filament thickness (measured in number of protofilaments). B, C, and E are the bending, twisting, and stretching moduli of an individual protofilament, respectively. For an actin bundle, the thickness dependence of bending and twisting ranges from linear (n) for slippery protofilaments to quadratic (n^2) for nonsliding protofilaments, with a cross-linker-dependent crossover [41]. For MreB, lateral interactions appear strong, so we assume a quadratic dependence on n.

By imposing the observed helical configuration we can use variational techniques to estimate the forces working against monomer addition at the filament tips. In Appendix A, we derive the force acting at the filament tips along the filament direction in the inextensible ($E \to \infty$) and freely twisting [$\tau(s)=0$] regimes:

$$F_B = \begin{cases} f_B \sin^2\theta(1+3\cos^2\theta)\langle n^2\rangle, & L_{fil} > L_c, \\ 0, & L_c > L_{fil}, \end{cases} \tag{5}$$

where θ is the pitch angle of the helix and $f_B \equiv B/2R_c^2 \approx 0.031$ pN is the elastic force scale. L_c and R_c are the length and radius of the cylindrical portion of the cell, respectively. If the bundle thickness $n(s)$ exhibits significant inhomogeneity, then the appropriate average thickness n is the root-mean-square average thickness along the bundle length. Other than the buckling point at $L_{fil}=L_c$, F_B is independent of L_{fil} for a given θ. The helical pitch p and pitch angle θ are related by

$$p = \frac{2\pi R_c}{\tan\theta}, \quad \cos\theta = \frac{L_c}{L_{fil}}. \tag{6}$$

As the pitch p vanishes, $\theta \to \pi/2$ and $F_B \to f_B n^2$. The force F_B has a maximum of $F_B^{\max} \equiv \frac{4}{3} f_B n^2$ at $\theta^* = \arctan\sqrt{2} \approx 0.96 \approx 55°$.

Many of our results reflect the fact that we work in a regime where elastic forces F_B and the polymerization force scale $f_0 \equiv k_B T/a_0 = 0.80$ pN are similar in magnitude.

III. RESULTS

A. Stochastic steady state

In a typical *B. subtilis* cell of volume 1.9 μm^3, only four unpolymerized monomers are necessary to achieve the critical concentration of MreB, $c_c = 0.003$ μM—suggesting that stochastic effects, due to the discrete molecular nature of the polymerizing monomers, may be significant. Similarly, the number of protofilaments in a typical cross section of the MreB helix is small (less than 20) and the number of protofilaments in contact with the cell wall at the helix tips, n_{tip}, is even smaller. A deterministic mean-field analysis of the steady state (see Appendix B), neglecting stochastic fluctuations, can be compared with fully stochastic simulations to explore the impact of various stochastic effects in this system.

We simulated n protofilaments that grew and shrank stochastically within a common pool of N_0 monomers according to the force-dependent polymerization rates, Eq. (1), and force-independent depolymerization rates. The forces on each protofilament tip were determined by the constraint

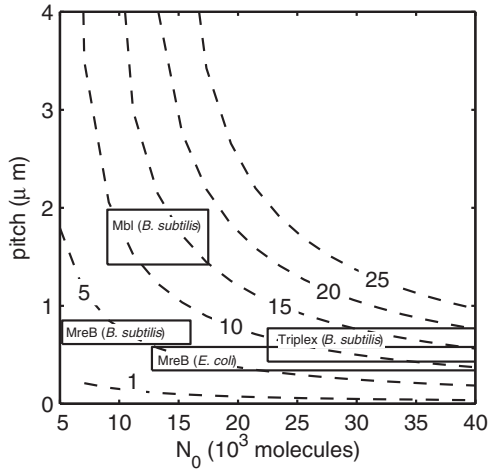

FIG. 2. Steady-state pitch p vs total molecule number N_0 for various filament bulk thicknesses n as predicted by stochastic simulation. The mean-field plot is indistinguishable from this due to the low cytoplasmic concentration. The rectangles represent approximate regions of experimental relevance from [7,9,14]. In *B. subtilis*, if the three isoforms bundle together into a nonslipping triplex structure, the number of monomers will be the sum of each homolog.

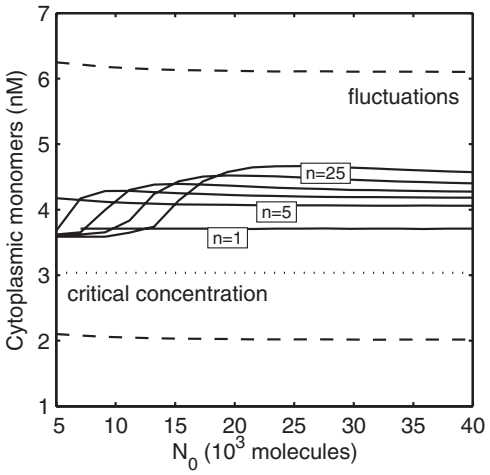

FIG. 3. Steady-state cytoplasmic concentration c of MreB monomers vs total monomer number N_0 from stochastic simulation for n protofilaments, showing $n=1$, 5, 10, 15, 20, and 25. The dotted line represents the critical concentration. The dashed line illustrates the large standard deviation of stochastic fluctuations in steady state, for $n=5$. For all n, relative fluctuations were $50\% \pm 5\%$ and absolute fluctuations were within 0.2 nM of those shown for $n=5$.

force on the bundle, Eq. (5), divided among the leading filaments at that tip, where $1 \leq n_{tip} \leq n$. The filament bundle was studied once it reached a steady state. The length of each of the n protofilaments and the monomer concentration continued to fluctuate within the steady state, as did the number of protofilament tips, n_{tip}, at a given end of the filament bundle.

For a given cell geometry (L_c and R_c) and total number of monomers (N_0), each bulk thickness n yields a unique helical steady-state configuration with a particular pitch p and average cytoplasmic monomer concentration c. As seen in Fig. 2, as the abundance N_0 increases for a given number of protofilaments n, the pitch decreases due to longer bundles. Conversely, at a given N_0, thicker bundles (larger n) leads to larger pitches.

The rectangles in Fig. 2 represent independent experimental measurements of MreB abundance and cable pitch in *B. subtilis* [7,14] and *E. coli* [9]. In *B. subtilis*, if the three MreB isoforms (MreB, Mbl, and MreBH) bundle together into a triplex structure, the total number of monomers should be the sum from each homolog, which we estimate is 23 000–40 000. We see that with current experimental pitch and abundance estimates, *E. coli* has $n \in [3,16]$ protofilaments in each polarized MreB helical bundle. Under the assumption that they are bundled independently of the other isoforms in *B. subtilis*, we estimate that Mbl has $n \in [9,21]$, while MreB has $n \in [3,7]$, with pitches from [7]. Under the assumption that the isoforms are mutually nonslipping, we estimate $n \in [8,21]$ in the triplex with the mutual pitch from [8]. It is therefore possible that the distinct pitches reported by [7] and [8] are the result of changes in the bundling properties of the variously labeled and tagged MreB analogs.

The concentration of MreB in monomeric form shown in Fig. 3 is low, representing less than 0.1% of the total cellular MreB. This is in contrast to the same model using eukaryotic actin kinetics, for which 1%–5% is monomeric (data not shown), and in dramatic contrast with observations of FtsZ polymerization, for which 30% is associated with the Z ring and 70% is diffuse in the cytoplasm *in vivo* [42]. Notwithstanding, the average monomeric concentration of MreB is significantly above the critical concentration due to a reduced polymerization rate which arises from the constraining force at the bundle tips. The shape of the curves in Fig. 3 follows from the force versus pitch relationship in Eq. (5), which grows quickly, reaches a maximum, and then decreases again as the pitch angle approaches $\pi/2$. As we shall see, force and cytoplasmic concentration increase together, while, as we have seen, pitch and N_0 are inversely related. As a result, for each n the cytoplasmic concentration exhibits a similar maximum versus N_0 as force does versus pitch. This maximum, corresponding to θ^*, is at larger N_0 for larger n. We also see in Fig. 3 that the fluctuations in the monomeric concentration are very large and approximately independent of n and N_0. The cell is often instantaneously below the critical concentration despite the upward bias due to the constraint forces.

As seen in Fig. 4(a), the maximal force F sustainable by the bundle in steady state increases with the cytoplasmic concentration c. For this part of the figure c was held fixed, to facilitate comparison with both the mean-field calculations in Appendix B and the stochastic $n=2$ calculations in Appendix C. The increase of F with c comes from Eq. (1), the force-induced reduction of the polymerization-rate, and reflects the excess of the monomer fraction over the critical concentration line seen in Fig. 3. F increases with the number of protofilaments, n, at a fixed cytoplasmic concentration, since it is distributed over the leading n_{tip} protofilaments. The excess of F over the *maximal* mean-field prediction (dashed lines), where $n_{tip}=n$, is recovered analytically for $n=2$ (solid line) in Appendix C. The excess arises because any

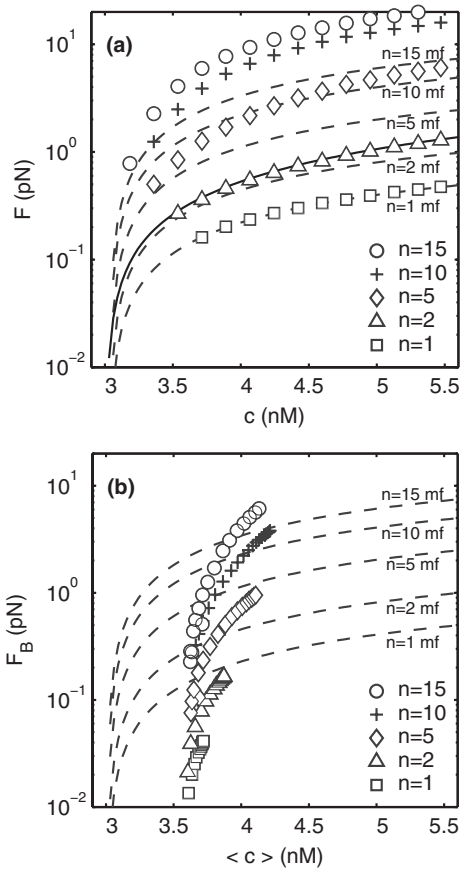

FIG. 4. Maximal steady-state force generation F by a filament bundle with a stochastic n_{tip} as a function of steady-state concentration c. Various average bundle thicknesses n are shown. The dashed lines represent the mean-field predicted force-concentration relation [Eq. (B1)] if $n_{tip}=n$ independent tips were all sharing the load. (a) We hold c fixed and allow an arbitrary bundle stiffness. The solid line represents the analytic prediction for $n=2$ with a stochastic n_{tip}. The points indicate stochastic simulations, only allowing n_{tip} to vary. Fluctuations in n_{tip} allow a significantly increased force compared to the mean-field results. (b) The points indicate fully stochastic simulations, for the same n as in (a), and the average c is used. A specific bundle elasticity is imposed by forcing $F=F_B$. Fluctuations in c systematically decrease the bundle force compared to (a), and this effect is stronger for smaller c.

of the n_{tip} protofilaments may grow and extend the bundle length, after which the remaining near-tip protofilaments will quickly catch up without force retardation. The result is enhanced growth at a given F or, equivalently, a larger F at which a steady state is reached. The stochastically-enhanced force is more significant as n increases and also increases with c due to the increased polymerization rate.

In Fig. 4(b), we examine the additional effects on F due to the large fluctuations in c that were apparent in Fig. 3. Here we plot F_B versus the average c for fully fluctuating filament bundles. Various c were explored by varying N_0. We include the mean-field results (dashed lines) for reference. Two differences with Fig. 4(a) are apparent. The first is that the fully fluctuating results have a maximal force sustainable by the elastic bundle, $F_B^{\max}=4/3f_Bn^2$. With c fixed we could use an arbitrarily stiff bundle to explore a wider range of forces, but

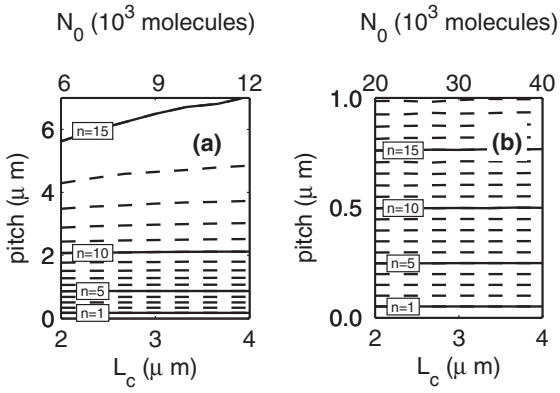

FIG. 5. Pitch p as the cell length L_c grows for various filament bulk thicknesses n_{bulk} as predicted by stochastic simulation, for (a) $N_0=3\times10^3L_c$, so that an average 3-μm cell contains 9000 MreB monomers, corresponding to regimes toward the low-N_0 end of Fig. 2, and (b) $N_0=10^4L_c$, corresponding to the high-N_0 end. For most bundle thicknesses, the pitch is effectively constant as the cell elongates. However, for thicker bundles in the low-N_0 regime, the helical pitch exhibits a significant dependence on the cell length, expanding as the cell doubles in size.

here we need to choose a particular stiffness (by equating $F=F_B$) to accurately couple fluctuations in c with those of F. The second difference is that F for the fully-fluctuating system is *below* the mean-field results for $n\leq5$ and is lower than the results in Fig. 4(a) for a fluctuating n_{tip}. This systematic decrease can be seen as arising from averaging the concave-down curves from Fig. 4 over the very large c fluctuations, which leads to a stronger decrease for smaller average c.

There are significant effects on the forces sustained by the filament bundle both due to fluctuations in the small number of protofilaments supporting the force at the bundle tip, n_{tip}, and due to the large fluctuations in the monomer concentration c. Because of the curvature of the F vs c curve, these fluctuation effects modify the mean-field steady-state bundle force in opposite directions. While for small numbers of protofilaments ($n\lesssim5$) the overall effect is to reduce F for a given c, the net effect for the physiological range of bundle thicknesses (Fig. 2) and cytoplasmic concentrations (Fig. 3) is an increased force.

B. Cell growth

The MreB helix grows as the cell grows, doubling its lateral length before dividing. Our quasistatic approach can accommodate cell growth. We assume that the total number of monomers N_0 is proportional to the cell length and that the number of protofilaments n is length independent. We simulated cell growth in a regime toward the low-N_0 end of Fig. 2, with $N_0=3\times10^3L_c$, so that an average 3-μm cell contains 9000 MreB monomers, and toward the high-N_0 end, with $N_0=10^4L_c$. Figure 5 shows how the steady-state helical pitch varies as the cell length L_c ranges between 2 and 4 μm.

For most bundle thicknesses n, the pitch is nearly constant as the cell elongates. However, for thicker bundles in the low-N_0 regime, the helical pitch increases significantly as the

cell doubles in size. This increase is due to fluctuations at small cell lengths L_c. While it appears strange that at *large n* the stochastic effects are larger, the pitch is determined by the filament length L_{fil}, which only depends on the maximum protofilament length. While the mean protofilament length fluctuates less with increasing n, the maximum protofilament length is an extremal property of the bundle—and increases with increasing n. At small L_c, the relative fluctuations in the cytoplasmic fraction also increase. For the larger-N_0 regime of Fig. 5(b), the pitches are much smaller, L_{fil} larger, and relative length fluctuations correspondingly smaller.

In the physiological regimes shown by boxes in Fig. 2, pitch should not change significantly during cell growth if the overall concentration of MreB monomers remains constant. Mbl in *B. subtilis* may have longer pitches in longer cells [11,15], though this is not a strong effect [7]. Experimental observations of considerable variability of the number of helical turns per cell within cells of the same strain, size, and growth conditions [11] may imply a corresponding variability of MreB expression or of the cross-sectional number of protofilaments n—which complicates analysis.

C. Macromolecule trafficking

A vital role of MreB is the polar localization of proteins such as Tar in *E. coli* [21], the cell polarity markers DivJ and PleC in *C. crescentus* [22], and the origin-proximal regions of the newly-replicated chromosome in *E. coli*, *B. subtilis* and *C. crescentus* [23]. One possibility is that these passengers associate with yet-to-be-discovered motor proteins that use MreB as a track to the poles [21]. A second possibility is that these proteins simply bind to the helix and advect with the continuous treadmilling, eventually ending up at one of the polar tips. A third possibility is that they associate with leading tips of MreB protofilaments [16], perhaps via intermediary proteins analogous to formin for actin filaments. Here we quantitatively analyze these possibilities, which are depicted in Fig. 6, together with associated translocation speeds with respect to the fixed bacterial axis.

For any transport mechanism, a characteristic speed along the filament bundle, v_{trans}, translates into a speed $v_z = \cos\theta v_{trans}$ relative to the cell's axis. Assuming the protein initially binds at a uniformly random location along the bundle, the average time to reach a pole is then

$$\langle t_{trans}\rangle \approx \frac{L_c}{2v_z} = \frac{L_c}{2\cos\theta v_{trans}}. \tag{7}$$

This time can be compared to the cell division time to see whether it provides a plausible mechanism for polar localization.

The myosins that transport organelles along actin tracks in eukaryotes travel at speed $v_{mot} \approx 200$–400 nm/s [43]. Attached to putative myosin homologs, macromolecules could be translocated to the poles in ~20 s. This is well within cell division times, so this would be a viable polarization mechanism. However, no cytoplasmic motor homolog has been identified in prokaryotic cells. Furthermore, almost all myosins travel toward the pointed ("+") tip along actin filaments [44], so a single polarized MreB bundle would probably only support motor-driven localization to one pole while unpolarized bundles would not support selective targeting to one pole and not the other.

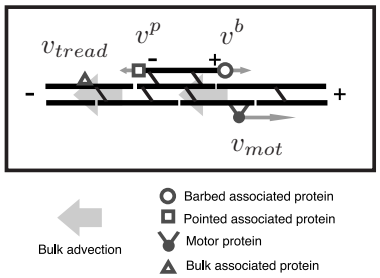

FIG. 6. Schematic of the different possible modes of transport along MreB bundles. Velocities are absolute with respect to the cell in the indicated directions. Bulk treadmilling advects bundles that span the cell length at a speed v_{tread} toward the slow-growing pointed ("–") end. Side associated protofilaments, without constraint forces at their tips, have different polymerization rates and so are not simply advected with the bundle. Their tip velocities are v_p and v_b for pointed and barbed ends, respectively. As discussed in the text, v_b is always opposite the treadmilling direction. Putative motor proteins would probably be polarized and would have a characteristic speed v_{mot}. The figure illustrates one polarized protofilament bundle; however, it is possible that two oppositely polarized bundles would exist within a cell—in which case the polarity and velocities of the second bundle should be opposite the first.

Static association of proteins to the side of MreB bundles would, through treadmilling, lead to a translocation speed equal to the rate of advection times the monomer spacing, $\lambda_{tread}a_0$, in the direction of the pointed end of the bundle. In a steady state, the advection rate $\lambda_{tread}=1.2\ s^{-1}$ is independent of the buckling force, the bundle thickness, or the cytoplasmic concentration and leads to $v_{tread}=a_0\lambda_{tread}=5.92$ nm/s, shown by the dashed line in Fig. 7(c). Applying Eq. (7) to a typical configuration with $p=1$ μm and $L_c=3$ μm, this yields $\langle t_{trans}\rangle \approx 12$ min, which is plausible compared to cell-division time scales and comparable to *oriC* translocation times [27].

Proteins that could bind either directly or via putative tip-binding proteins (analogous to formin in eukaryotes [16,45]) to the barbed end of free protofilaments could be translocated in the *opposite* direction to the treadmilling advection. In an unbuckled ($F_B=0$) filament, lateral protofilaments treadmill at the same rate of the net backward advection of the bundle, accomplishing no net movement relative to the cell's axis. In a buckled filament, however, the monomer concentration is considerably above the critical concentration of a free protofilament, as illustrated in Fig. 3. As a result, unconstrained laterally associated barbed ends grow faster than the bulk of the bundle, with

$$v_b = a_0[(k^b_{\rm on}c - k^b_{\rm off}) - \lambda_{tread}] = a_0 k^b_{\rm on}(c - c_c). \tag{8}$$

For each bundle thickness and pitch simulated, the translocation times are shown in Fig. 7(a) and speeds in Fig. 7(c). Typical bundles with 20 000–40 000 molecules of MreB and 8–15 protofilaments thick would transport passengers in 4–6

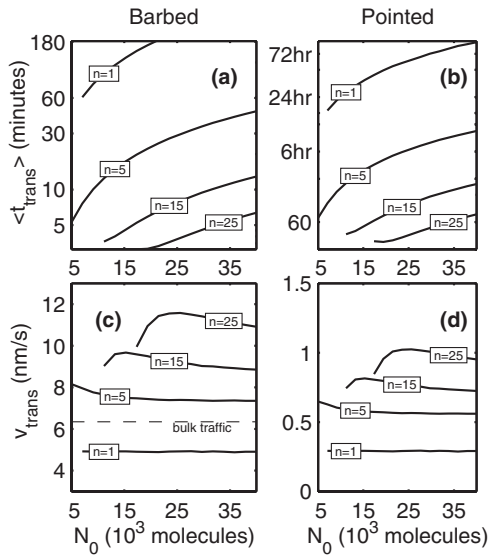

FIG. 7. Mean translocation times $\langle t_{trans} \rangle$ for macromolecule passengers being transported by MreB side protofilaments treadmilling on the side of the main cables vs N_0. Constraint forces at the ends of the helix keep c above c_c, so that significant axial movement can be seen with respect to bulk treadmilling. Different modes of transport along the cables are depicted schematically in Fig. 6. Barbed ends move antiparallel with respect to bulk advection (a),(c). Pointed ends move in the same direction as bulk advection; however, the slower polymerization rates lead to much longer translocation times (b),(d). Lateral traffic associated with parts of the bulk cables move toward the pointed end at $a_0\lambda_{tread}$, indicated in (c) by the dashed line. Any passenger dissociation and reassociation from protofilament tips will increase the translocation times and decrease the effective speeds.

min, considerably faster than laterally-associated proteins and in the opposite direction.

Proteins associated with the slow-growing pointed end have a net velocity given by

$$v_p = a_0[(k_{\text{on}}^p c - k_{\text{off}}^p) + \lambda_{tread}] = a_0 k_{\text{on}}^p (c - c_c). \tag{9}$$

Note that free pointed ends are *disassembling* on average, though not as rapidly as the treadmilling, so that $0 < v_p < v_{tread}$. These translocation times are shown in Fig. 7(b) and speeds in Fig. 7(d). According to Eqs. (8) and (9), they are slower by a factor of $k_{\text{on}}^b / k_{\text{on}}^p \approx 10$ compared to free barbed ends, taking several hours. These times are probably too slow to be biologically relevant.

These protofilament-associated translocation modes offer a non-motor-based mechanism for specific targeting of proteins to *either* pole in cells with a single polarized bundle of MreB. The cell could specify the specific pole destination of a particular protein by specifying which part of an MreB protofilament it binds to: barbed-associated proteins would end up at the pole at the barbed-tip of the MreB bundle with a speed of v_b, while laterally-associated proteins would end up at the pointed-tip pole with speed $v_{tread} = a_0\lambda_{tread}$. Of course, these translocation mechanisms may also supplement a (hitherto undiscovered) motor-based mechanism to provide targeting to either pole with polarized MreB bundles. We do not see any way of specific targeting of proteins to a given pole if the MreB bundle is not polarized or if there are antiparallel bundles, either with or without motor proteins.

If protofilaments dissociate at a significant rate from the main bundles, then these translocation times represent lower bounds. Additionally, any putative MreB-binding proteins could strongly affect the polymerization kinetics. For example, ADF/cofilin in eukaryotes increase k_{off}^p for actin by $\sim$20 times. A bacterial homolog of such a protein would decrease the delivery time of pointed-associated proteins by $\sim$20. Similarly, in the presence of profilin, formin increases the barbed growth rate of actin by 10- to 15-fold [46], and such a modification would decrease the delivery time of barbed-associated proteins to within a minute.

Proteins associated with pointed or barbed ends of protofilaments could be translocated toward those poles at v_p and v_b, respectively. However, the proteins could also be directly recruited to distinct poles of the cell, due to the free ends of the MreB bundles. The relative magnitude of translocation versus direct recruitment is dependent on the number of barbed or pointed protofilament ends. Tip-associated translocation requires a significant number of laterally associated protofilaments tips to maximize the translocation flux, while tip-directed polar recruitment requires unbroken protofilaments to minimize nonpolar binding sites. Observations in *C. crescentus* [10] indicate that protofilaments are short, supporting tip-associated translocation as a viable mechanism *in vivo*.

D. Recovery dynamics of helices

In experiments on *B. subtilis* involving fluorescence recovery after photobleaching (FRAP) of fluorescence-tagged Mbl, four helical turns on one side of the cell's longitudinal axis were bleached while the other half continued to fluoresce. It took approximately 8 min for the bleached halves to recover fluorescence at the same level as the unbleached halves [15]. We obtain an upper bound for this time by calculating the average time unbleached parts of the MreB protofilaments take to treadmill into the bleached regions: one half-turn in the polarized model and one quarter-turn in the nonpolarized models. Thus, in silico,

$$t_{FRAP} \approx \frac{\pi R_c}{a_0 \sin\theta \lambda_{tread}} = \frac{\pi\sqrt{p^2 + R_c^2}}{a_0 \lambda_{tread}} \tag{10}$$

for polarized array structures and half of that for nonpolarized array structures. For $p \approx 0.5$ μm this yields between 3 and 6 min. The agreement of this time scale with experiment suggest that monomer renewal by exchange with the cytoplasm may not dominate the FRAP recovery time.

Several experiments have applied the MreB-specific small molecule A22 to quickly and reversibly break down the MreB cytoskeleton by blocking polymerization [23,25]. Cells remain viable after recovery from A22-induced disruption of MreB and reform their helical patterns in less than 1 min for *C. crescentus* [25]. In the context of our model, recovery from A22-treatment corresponds to the reestablishment of the steady-state MreB helix from a pool of cytoplasmic monomers. We simulated our stochastic model from a

nucleus of n protofilaments, each of length 3 (as suggested for actin [47]), under the assumption that the nucleation time is short [31]. Thicker bundles (larger n) reach their final steady-state length much faster than thin bundles, due to the presence of more free filament ends. The equilibration times vary between 1 and 5 s. Fewer bundled protofilaments took longer to reach a steady state, the longest being $n=1$, with $N_0=10\,000$, in which the final length is reached in 5 s. These are consistent with A22 recovery time scales.

We can also address the time scale of breakdown. Assuming that A22 simply blocks polymerization, but does not change the depolymerization dynamics, then it will take $t_1=L_{fil}/(k_{\mathrm{off}}^p+k_{\mathrm{off}}^b)\approx 13$ min for each protofilament to disassemble with no internal free ends. If each protofilament has length L_{proto} with $m=L_{fil}/L_{proto}$ free pointed (or barbed) ends, then we would expect the disassembly to be correspondingly faster, with $t_m=t_1/m$. Experiments constrain the actual disassembly time in *C. crescentus* [25] to be ≤ 1 min, implying $m\geq 13$ and $L_{proto}\approx 300$ nm. Analysis of single-molecule experiments in *C. crescentus* estimates $L_{proto}\approx 392\pm 23$ nm [10] by assuming that protofilaments treadmill in place. If protofilaments also advect along the bulk MreB cable, as we assume in our model, this experimental estimate represents an upper bound and is consistent with our result.

These estimates of assembly and disassembly time scales of the MreB helix can also be applied to the reported midcell condensation of MreB in *E. coli* [12] and *C. crescentus* [13], and of MreBH in *B. subtilis* [42]. Two possible mechanisms are an elastic compression of the intact MreB helix to midcell driven by some (posited) motor protein or disassociation of the MreB helix and (transient) association with some midcell binding partners. These mechanisms may occur in tandem. The time scales of condensation and recovery are ≈ 30 min in *C. crescentus* which is considerably longer than A22-induced breakdown. The maximum filament-end force needed to compress a typical MreB helix in our model from L_c to a midcell spiral is $F_B^{\max}\approx 10$ pN and is comparable to the force generated by the RNA polymerase [23] and the anchoring forces of integral membrane proteins [48]. Thus, both motor-driven compression and depolymerization are plausible mechanisms for the observed midcell condensation.

IV. DISCUSSION

Our model explains how polymerization forces in a bundle of MreB protofilaments can maintain a helical configuration in mechanical equilibrium. Helices are observed increasingly often within bacteria [4], and our model suggests an elastic mechanism for maintaining such helicity when filament bundles extend the length of the cell. For MreB, our model predicts that the observed pitches and protein abundance are consistent with bundles of 10–20 protofilaments thick.

Helical pitch is directly observable through fluorescence microscopy, and the total abundance of MreB can be controlled by an inducible promoter [15]. Increasing the MreB expression level should systematically decrease the pitch according to the curves in Fig. 2. We have assumed a cytoplasmic pool of monomers, while there is evidence of an oligomeric pool of Mbl in *B. subtilis* [15]. Since only monomers will contribute to force-generation through polymerization, an oligomeric pool that was not part of the MreB bundle would simply lead to a shift along the N_0 axis in Figs. 2 and 3.

Filament treadmilling is ongoing in the steady state. A significant result is that parts of the filament may travel faster than the bulk treadmilling rate, even in the opposite direction, while other parts may travel much slower. Since the cytoplasmic concentration is held above the critical concentration of free protofilaments by the constraining forces at the filament tips, the barbed end of protofilaments that associate laterally with the MreB bundles can travel at speeds greater than the bulk advection speed. These speeds are fast enough to be biologically relevant in the transport of polar-targeted proteins and the origin-proximal part of the chromosome. These transport modes may explain how MreB cables transport passengers without motor proteins and may also reconcile experimental observations of very different speeds of MreB protofilaments: fast speeds of 0.07 μm/s [11] may correspond to the lateral protofilaments described above, while slow speeds comparable to actin treadmilling speeds [10] may correspond to protofilaments involved in the bulk of the cables. It also suggests that observations of bidirectional transport along MreB cables [10] do not necessarily rule out a single polarized MreB bundle.

It has been suggested that cell polarity arises from the inherent polarity of MreB polymers [16,22]. The different modes of transport in our model provide a mechanism for translating the polarity of a cable to the entire cell. We propose that proteins destined for one pole associate laterally with the cable and are naturally translocated toward the "pointed" pole. Proteins destined for the other pole bind to the barbed ends of free protofilaments and are naturally translocated toward the "barbed" pole. We have demonstrated that such translocation happens within a physiologically relevant time scale. Such selective targeting requires polarized MreB filaments. Proper polarization of the MreB cables themselves may require an upstream nucleator, for which TipN in *C. crescentus* is a candidate [49]. While antiparallel MreB cables can support transport to both poles, we do not see how it can support targeted transport to specific poles.

Evidence for polarity of MreB in *C. crescentus* is mixed [10,22]; however, both PleC and DivJ appear to have targeted localization to specific poles during the cell cycle [23]. This is consistent with a single polarized MreB cable in *C. crescentus*. We are not aware of evidence about MreB cable polarization in *E. coli*. While FRAP recovery of Mbl cables in *B. subtilis* is symmetric [15], this could be due to lateral exchange and/or the motion of laterally associated protofilaments.

Any transport along treadmilling MreB bundles would require either direct association of targeted proteins with MreB or association through an intermediary. Interactions of only a few cytoplasmic proteins with MreB have been identified. These include SetB, implicated in chromosome segregation [24], RNA polymerase [23], and the chaperonin GroEL [23]. Of these, GroEL is known to interact with a large number of

cytoplasmic proteins [50], while RNA polymerase is needed for their transcription. GroEL is localized to polar and septal regions in *E. coli* [51] while RNAP is associated with nucleoids in punctate patterns similar to those seen for helically distributed proteins [52,53]. It would be interesting to see if any of these MreB-associated cytoplasmic proteins exhibit pole-directed transport within bacterial cells.

Transport speeds may be decreased if short protofilaments necessitate multiple binding and release events to translocate from one pole to the other. Tip-directed transport also allows for direct recruitment to free protofilament tips, such as at the bundle ends. The details of bundle ultrastructure and of protein translocation will be required to sort out these competing effects.

We have shown that many of the dynamical phenomena associated with MreB, including polar protein localization, MreB helix dissolution and reformation, and FRAP studies, could result from polymerization and treadmilling of bundled MreB protofilaments without motor proteins. In order to make precise quantitative predictions, direct measurements of the kinetic rate constants for MreB polymerization would be invaluable. The *Thermotoga*-scaled MreB parameters that we used are consistent with experiment and require the least amount of *ad hoc* parameter adjustment. Pitch-abundance and concentration-abundance relationships did not change in character between eukaryotic actin and our *Thermotoga*-scaled MreB kinetics. Conversely, translocation times and time scales for dissolution and reformation of MreB helices are strongly parameter dependent. However, our qualitative result of bidirectional transport is general since, from Eq. (8), v_b is always in the opposite direction from the bulk treadmilling.

There are two significant sources of stochastic effects in our model. Stochastic fluctuations due to the number of force-bearing protofilaments, n_{tip}, significantly increase the net force applied to the bundle [Fig. 4(a)]. There are also large fluctuations in the cytoplasmic monomer concentration in the steady-state, c (Fig. 3), and these systematically *decrease* the net forces [Fig. 4(b)]. We have shown that the stochastic effects of c, due to the small cell volume combined with the low critical concentration, and the stochastic effects of n_{tip}, due to the relatively small number of protofilaments, are both significant.

We have assumed that MreB polymers are naturally straight, without intrinsic curvature or twist. There are suggestions that MreB helices are always right handed [7]. Handedness could result from nucleation conditions or constraints at the helix ends, which would not affect our results. Handedness could also arise from a nonzero intrinsic twist τ_o in Eq. (4). For small $|\tau_o| \ll R_c^{-1}$, the elastic force in Eq. (5) would remain unaffected. It has been hypothesized that MreB exhibits an anisotropic membrane affinity requiring one face of the monomers to always orient toward the membrane together with significant intrinsic curvatures [54]. If so, our polymerization dynamics could still be applied though with a more complex energy functional [54]. However, we would expect qualitatively similar results if helical extension remains force limited.

We have demonstrated that many of the dynamical phenomena associated with MreB, including polar protein localization, MreB helix dissolution and reformation, and FRAP studies, can be addressed by polymerization and treadmilling of bundled MreB protofilaments without the need to invoke motor proteins. The study of the MreB helix ultrastructure, as well as the detailed study of the translocation of MreB-associated pole-directed proteins in the various bacterial species with various MreB analogs, will shed further light on the viability of our results *in vivo*.

We thank NSERC for financial support and Rut Carballido-Lopez for discussions.

APPENDIX A: GLOBAL ELASTICITY MODEL

Following Antman [40], an elastic filament is described by the position of its centerline $\vec{r}(s)$ and an orthonormal basis of directors $\{\vec{d}_1(s), \vec{d}_2(s), \vec{d}_3(s)\}$ specifying the orientation of its cross section. This approach has been used extensively for DNA [39], but is seldom used for eukaryotic actin (though see [55]) since actin does not systematically form structures *in vivo* that are much smaller than its persistence length. In contrast, MreB forms a helix with a radius of ≈ 400 nm, which is smaller than the persistence length of a single protofilament ($\xi_p = B/k_B T \approx 15$ μm) and much smaller than ξ_p for a bundle of several protofilaments.

The stretching modulus of a filament bundle of actin is $nE \approx 40n$ pN where n is the number of protofilaments in a typical cross section of the bundle. For a typical filament with $n=15$, the energy scale to stretch the filament by monomer addition is $\Delta U_{stretch} = Ena_0 \approx 2 \times 10^3$ pN nm, whereas a comparable energy scale for bending the helix is $\Delta U_{bend} = Ba_0/4R_c^2 n^2 \approx 70$ pN nm. We therefore assume that the MreB filament bundle is inextensible and parametrize the filament by its arclength $s \in [0, L_{fil}]$. The angular strains in the filament are then simply $\partial_s \vec{d}_i = \vec{u} \times \vec{d}_i$, $\vec{u} = \kappa_1 \vec{d}_1 + \kappa_2 \vec{d}_2 + \tau \vec{d}_3$ where $\kappa^2 \equiv \kappa_1^2 + \kappa_2^2$ is the curvature and τ is the local twist. We set $\vec{d}_3 \equiv \partial_s \vec{r}$, following the standard shear-free assumption of biopolymers.

The centerline of a helix with pitch angle θ (measured from the cell's axis $\hat{z}$) and radius R_c is

$$\vec{r}(s) = R_c \cos\left(\frac{\sin\theta}{R_c} s\right)\hat{x} + R_c \sin\left(\frac{\sin\theta}{R_c} s\right)\hat{y} + \cos\theta s \hat{z}. \tag{A1}$$

Using the tangent, normal, and binormal unit vectors $\{\vec{t}(s), \vec{n}(s), \vec{b}(s)\}$ and the Frenet-Serret theorem [40], we obtain the curvature of the helix,

$$\kappa = \frac{\sin^2\theta}{R_c}, \tag{A2}$$

and the torsion of the filament's centerline,

$$\tau_c = \frac{1}{R_c} \cos\theta \sin\theta. \tag{A3}$$

The directors $\{\vec{d}_1(s), \vec{d}_2(s)\}$ are, in general, a rotation of $\{\vec{n}(s), \vec{b}(s)\}$ through an angle $\phi(s)$. The difference between

the physically relevant total twist τ and the centerline torsion τ_c is $\tau_L \equiv \tau - \tau_c = \partial_s \phi$ [56].

Using the elastic energy from Eq. (4) and $L_c = L_{fil} \cos\theta$ and assuming that τ_L is free to rotate to eliminate $\tau(s)$, we find

$$\frac{\partial \mathcal{H}}{\partial L_c} = -\frac{2B}{R_c^2} \sin^2\theta \cos\theta \langle n^2 \rangle, \tag{A4}$$

$$\frac{\partial \mathcal{H}}{\partial R_c} = -\frac{BL_{fil}}{R_c^3} \sin^4\theta \langle n^2 \rangle, \tag{A5}$$

$$\frac{\partial \mathcal{H}}{\partial L_{fil}} = -\frac{B}{2R_c^2} \sin^2\theta (1 + 3\cos^2\theta) \langle n^2 \rangle. \tag{A6}$$

Regardless of any mechanisms holding the MreB bundle in a helical configuration, one additional monomer must provide an energy of $(-a_0 \partial \mathcal{H}/\partial L_{fil})$ to polymerize itself to the tip of the longest protofilament(s). This provides an estimate for the force acting upon the tip of the filament bundle,

$$F_B = \begin{cases} f_B \sin^2\theta (1 + 3\cos^2\theta) \langle n^2 \rangle, & L_{fil} > L_c, \\ 0, & L_{fil} < L_c, \end{cases} \tag{A7}$$

where $f_B \equiv B/2R_c^2 \approx 0.031$ pN. This implies that $F_B \approx 10$ pN for $n \approx 10$. This is comparable to pull-out forces of integral membrane proteins [48].

Equation (A4) provides an estimate for the force generated by the MreB cytoskeleton against the cell's end caps. An estimate for the difference in longitudinal spring constant of the cell with and without a properly formed MreB helix is

$$\Delta k_{cell} \approx \frac{\partial^2 \mathcal{H}}{\partial L_c^2} = \frac{2B}{L_c R_c^2} \cos\theta (3\cos\theta - 1) n^2. \tag{A8}$$

For $p = 1$ μm and $n = 15$, this yields 4×10^{-4} pN/nm. For *E. coli*, the spring constant of the entire cell is $\approx 10^3$ pN/nm [57] and is much larger for *B. subtilis*; thus, the spring constant differential provided by the MreB helix is insignificant. Similarly, Eq. (A5) provides an estimate for the radial line pressure the helix exerts on the lateral walls:

$$\frac{F_{\hat{r}}}{L_{fil}} \approx \frac{B}{R_c^3} \sin^4\theta n^2. \tag{A9}$$

For $p = 1$ μm and $n = 15$, this yields 0.03 pN/nm. Equation (A9) represents a force contrast between pushing the cell wall directly above the helix and elsewhere. A bundle with $n = 15$ has approximate thickness $a_0\sqrt{n} \approx 20$ nm and the local excess pressure over the cables is $\approx 5 \times 10^{-3}$ pN/nm^2. In comparison, turgor pressure inside *E. coli* has been measured at ≈ 0.1 pN/nm^2 [57], indicating that the rigidity of the MreB bundles does not directly provide significant structural support for the cell well.

We may also use the elastic model to check the self-consistency of our quasistatic helical configuration, Eq. (A1). At physiological temperatures, all cellular components undergo thermal fluctuations of the order $k_B T$. However, a typical helical bundle with $n = 5$ and $p = 1$ μm has an elastic energy of $U = 3.5 \times 10^5$ pN nm $\gg k_B T = 4.1$ pN nm. We therefore assume that the helical pitch does not significantly fluctuate due to thermal effects. An estimate for the time scale for elastic reorganization of the MreB helix can also be obtained from the relaxation time of the lowest hydrodynamic mode in the filament [58],

$$t_{elastic} \sim \frac{2^6}{(3\pi)^4 \ln 2} \frac{\eta L_{fil}^4}{B} \approx 0.02 \text{ s}, \tag{A10}$$

where η is the cytoplasmic viscosity. In comparison, the characteristic time for polymer elongation is given by the steady-state treadmilling rate,

$$t_{poly} \sim \frac{1}{\lambda_{tread}} = \frac{k_{on}^p + k_{on}^b}{k_{off}^p k_{on}^b - k_{off}^b k_{on}^p} \approx 1.7 \text{ s}. \tag{A11}$$

Since $t_{elastic} \ll t_{poly}$ we can assume that elastic relaxation is fast compared to the polymerization dynamics of interest.

APPENDIX B: MEAN-FIELD STEADY STATE

By neglecting stochastic fluctuations, we can analytically relate pitch, total monomer number, and cytoplasmic concentration. The two essential ingredients are stationary filament lengths due to treadmilling in the presence of elastic constraint forces and conservation of the monomer number. If $n_{tip} \in [1, n]$ protofilaments reach each tip, then, from Eqs. (1), (2), and (5),

$$F_B = f_0 \ln\left(\frac{c}{c_c}\right) n_{tip} = f_B \sin^2\theta (1 + 3\cos^2\theta) \langle n^2 \rangle. \tag{B1}$$

We also have conservation of the total number of monomers,

$$N_0 = N_A c + \langle n \rangle \frac{L_c}{a_0} \frac{1}{\cos\theta}, \tag{B2}$$

where N_0 is the total number of monomers, N_A is the number of molecules per μM for a given cell volume, and $\langle n \rangle$ is averaged along the length of the helix. Together these equations give a relationship between concentration and pitch angle,

$$\ln\left(\frac{c}{c_c}\right) n_{tip} = \frac{f_B}{f_0} \sin^2\theta (1 + 3\cos^2\theta) \left((N_0 - N_A c)^2 \frac{a_0}{L_c}^2 \cos^2\theta \right), \tag{B3}$$

and an equivalent relationship between bulk thickness and pitch angle,

$$\ln\left(\frac{N_0}{N_A c_c} - \langle n \rangle \frac{L_c}{a_0 N_A c_c} \frac{1}{\cos\theta}\right) n_{tip} = \frac{f_B}{f_0} \sin^2\theta (1 + 3\cos^2\theta) \langle n^2 \rangle. \tag{B4}$$

The mean-field force-concentration relation obtained from Eqs. (B1) and (B4) is plotted in Fig. 4 for $n_{tip} = n$, which maximizes F_B for the bundle.

APPENDIX C: STOCHASTIC BUNDLE TIP, $n_{bulk} = 2$

If a force F is applied to both ends of a protofilament, both k_{on}^b and k_{on}^p will be reduced by a factor of $\epsilon \equiv e^{-F/f_0}$

[30,34]. Though the treadmilling rate is unaffected by the forcing, the treadmilling concentration becomes

$$c = \left(\frac{k_{\text{off}}^b + k_{\text{off}}^p}{k_{\text{on}}^b + k_{\text{on}}^p} \right) e^{F/f_0}. \tag{C1}$$

In the absence of forces, every protofilament of a bundle treadmills with equivalent rates and critical concentrations. However, force generation by a bundle in which the load is applied only on the most advanced n_{tip} protofilaments behaves differently. Lagging filament tips grow without force retardation and with a reduced treadmilling concentration, thereby catching up to the tip more often than otherwise—increasing n_{tip} and reducing the load per loaded filament. This leads to a larger total load for the bundle for the same monomer concentration c. A similar effective increase in force generation due to stochastic fluctuations has been noted in passing [59], although not analyzed in detail. Here we explicitly work out the details for $n=2$. For $n>2$, the effects of force generation by a stochastic n_{tip} are expected to be even more significant, as is seen in Fig. 4.

We parametrize the system of two filaments by $i \in \{0,1,\ldots\}$, the number of monomer spacings between the two tips. For any i, two competing Poisson events could increase the spacing: addition at the leading tip and dissociation at the lagging tip. Reduction of i occurs by the complementary two events. The master equations lead to the following equations for stationary probabilities p_i:

$$i \geq 2{:}p_{i-1}(k_{\text{off}} + k_{\text{on}} c\epsilon) + p_{i+1}(k_{\text{on}} c + k_{\text{off}}) = p_i(k_{\text{off}} + k_{\text{on}} c\epsilon + k_{\text{on}} c + k_{\text{off}}),$$

$$i = 1{:}2p_0(k_{\text{off}} + k_{\text{on}} c\sqrt{\epsilon}) + p_2(k_{\text{on}} c + k_{\text{off}}) = p_1[2k_{\text{off}} + k_{\text{on}} c(1 + \epsilon)],$$

$$i = 0{:}2p_0(k_{\text{off}} + k_{\text{on}} c\sqrt{\epsilon}) = p_1(k_{\text{on}} c + k_{\text{off}}).$$

The factors of $\sqrt{\epsilon}$ arise when $i=0$ and there are two leading tips sharing the load, halving the force per filament. These equations lead to recurrence relations for p_i. Although i cannot exceed the length of the filament, the p_i vanish exponentially as i increases so we approximate $i_{\max}=\infty$. Imposing normalization $\Sigma p_i = 1$, we find

$$p_0^b = \frac{c(1-\epsilon)}{c(1+2\sqrt{\epsilon}-\epsilon)+2c^b}, \tag{C2}$$

where $c^b \equiv k_{\text{off}}^b / k_{\text{on}}^b$. An equivalent expression for p_0^p applies for the pointed end. The average polymerization velocity for these stationary probabilities is

$$\lambda^b = (2k_{\text{on}}^b c\sqrt{\epsilon})p_0 + (k_{\text{on}}^b c\epsilon - k_{\text{off}}^b)(1-p_0) = (k_{\text{on}}^b c\epsilon - k_{\text{off}}^b) + [k_{\text{on}}^b c(2\sqrt{\epsilon}-\epsilon) + k_{\text{off}}^b]p_0 \tag{C3}$$

and is a nontrivial function of both c and F (through ϵ). To solve for the treadmilling concentration at a given force, we insert the barbed and pointed equivalent versions of Eq. (C3) into $\lambda^p = -\lambda^b$, which is a cubic polynomial in c, and we extract the one real, stable root.

The relation between the total applied force F_B and the cytoplasmic monomer concentration c is shown by the solid line in Fig. 4. Note that this derivation (and the simulations in Fig. 4) imposes a static c, though n_{tip} fluctuates. The disagreement with the mean-field result (dashed line) indicates that the n_{tip} fluctuations are important for the total force.

[1] B. Alberts, D. Bray, J. Lewis, M. Raff, and K. Roberts, *Molecular Biology of the Cell*, 4th ed. (Garland Science, New York, 2002).

[2] K. A. Michie and J. Lőwe, Annu. Rev. Biochem. **75**, 467 (2006).

[3] J. Møller-Jensen, J. Borch, M. Dam, R. Jensen, P. Roepstorff, and K. Gerdes, Mol. Cell **12**, 1477 (2003).

[4] R. Carballido-Lopez, Microbiol. Mol. Biol. Rev. **70**, 888 (2006).

[5] Y.-L. Shih and L. Rothfield, Microbiol. Mol. Biol. Rev. **70**, 729 (2006).

[6] R. A. Daniel and J. Errington, Cell **113**, 767 (2003).

[7] L. J. F. Jones, R. Carballido-Lopez, and J. Errington, Cell **104**, 913 (2001).

[8] H. J. Defeu Soufo and P. L. Graumann, Mol. Microbiol. **62**, 1340 (2006).

[9] T. Kruse, J. Møller-Jensen, A. Løbner-Olesen, and K. Gerdes, EMBO J. **22**, 5283 (2003).

[10] S. Y. Kim, Z. Gitai, A. Kinkhabwala, L. Shapiro, and W. E. Moerner, Proc. Natl. Acad. Sci. U.S.A. **103**, 10929 (2006).

[11] H. J. Defeu Soufo and P. L. Graumann, EMBO Rep. **5**, 789 (2004).

[12] Y.-L. Shih, T. Le, and L. Rothfield, Proc. Natl. Acad. Sci. U.S.A. **100**, 7865 (2003).

[13] R. M. Figge, A. V. Divakaruni, and J. W. Gober, Mol. Microbiol. **51**, 1321 (2004).

[14] R. Carballido-López, A. Formstone, Y. Li, S. D. Ehrlich, P. Noirot, and J. Errington, Dev. Cell **11**, 399 (2006).

[15] R. Carballido-Lopez and J. Errington, Dev. Cell **4**, 19 (2003).

[16] A. Fiebig and J. A. Theriot, Proc. Natl. Acad. Sci. U.S.A. **101**, 8510 (2004).

[17] We use "protofilament" as a single polymerized strand of MreB monomers and "bundle" as one or more laterally associated protofilaments, while "filament" and "cable" are generic terms for similar structures.

[18] H. P. Erickson, Nature (London) **413**, 30 (2001).

[19] A. Formstone and J. Errington, Mol. Microbiol. **55**, 1646 (2005).

[20] C. W. Wolgemuth, Y. F. Inclan, J. Quan, S. Mukherjee, G. Oster, and M. A. R. Koehl, Phys. Biol. **2**, 189 (2005).

[21] Y.-L. Shih, I. Kawagishi, and L. Rothfield, Mol. Microbiol. **58**, 917 (2005).

[22] Z. Gitai, N. Dye, and L. Shapiro, Proc. Natl. Acad. Sci. U.S.A. **101**, 8643 (2004).

[23] T. Kruse, B. Blagoev, A. Løbner-Olesen, M. Wachi, K. Sasaki, N. Iwai, M. Mann, and K. Gerdes, Genes Dev. **20**, 113 (2006).
[24] O. Espeli, P. Nurse, C. Levine, C. Lee, and K. Marians, Mol. Microbiol. **50**, 495 (2003).
[25] Z. Gitai, N. A. Dye, A. Reisenauer, M. Wachi, and L. Shapiro, Cell **120**, 329 (2005).
[26] A. Karczmarek, R. M.-A. Baselga, S. Alexeeva, F. G. Hansen, M. Vicente, N. Nanninga, and T. den Blaauwen, Mol. Microbiol. **65**, 51 (2007).
[27] C. D. Webb, P. L. Graumann, J. A. Kahana, A. A. Teleman, P. A. Silver, and R. Losick, Mol. Microbiol. **28**, 883 (1998).
[28] A. Mogilner and G. Oster, Curr. Biol. **13**, R721 (2003).
[29] T. D. Pollard and G. G. Borisy, Cell **112**, 453 (2003).
[30] A. Mogilner and G. Oster, Biophys. J. **71**, 3030 (1996).
[31] O. Esue, D. Wirtz, and Y. Tseng, J. Bacteriol. **188**, 968 (2006).
[32] D.-J. Scheffers, L. J. F. Jones, and J. Errington, Mol. Microbiol. **51**, 749 (2004).
[33] F. van den Ent, L. Amos, and J. Löwe, Nature (London) **413**, 39 (2001).
[34] A. Mogilner and L. Edelstein-Keshet, Biophys. J. **83**, 1237 (2002).
[35] L. Edelstein-Keshet and G. Ermentrout, J. Math. Biol. **40**, 64 (2000).
[36] G. I. Bell, Science **200**, 618 (1978).
[37] T. S. Karpova, J. G. McNally, S. L. Moltz, and J. A. Cooper, J. Cell Biol. **142**, 1501 (1998).
[38] T. Kruse, J. Bork-Jensen, and K. Gerdes, Mol. Microbiol. **55**, 78 (2005).
[39] N. Chouaieb, A. Goriely, and J. H. Maddocks, Proc. Natl. Acad. Sci. U.S.A. **103**, 9398 (2006).
[40] S. S. Antman, *Nonlinear Problems of Elasticity*, 2nd ed. (Springer, New York, 2004).
[41] C. Heussinger, M. Bathe, and E. Frey, Phys. Rev. Lett. **99**, 048101 (2007).
[42] J. Stricker, P. Maddox, E. D. Salmon, and H. P. Erickson, Proc. Natl. Acad. Sci. U.S.A. **99**, 3171 (2002).
[43] M. Rief, R. S. Rock, A. D. Mehta, M. S. Mooseker, R. E. Cheney, and J. A. Spudich, Proc. Natl. Acad. Sci. U.S.A. **97**, 9482 (2000).
[44] A. L. Wells, A. W. Lin, L.-Q. Chen, D. Safer, S. M. Cain, T. Hasson, B. O. Carragher, R. A. Milligan, and H. L. Sweeney, Nature (London) **401**, 505 (1999).
[45] D. Kovar and T. Pollard, Nat. Cell Biol. **6**, 1158 (2004).
[46] E. C. Garner, C. S. Campbell, and R. D. Mullins, Science **306**, 1021 (2004).
[47] L. Edelstein-Keshet and G. Ermentrout, Bull. Math. Biol. **60**, 449 (1998).
[48] E. Evans, D. Berk, and A. Leung, Biophys. J. **59**, 838 (1991).
[49] H. Lam, W. B. Schofield, and C. Jacobs-Wagner, Cell **124**, 1011 (2006).
[50] W. Houry, D. Frishman, C. Eckerskorn, F. Lottspeich, and F. U. Hartle, Nature (London) **402**, 147 (1999).
[51] H. Ogino, M. Wachi, A. Ishii, N. Iwai, T. Nishida, S. Yamada, K. Nagai, and M. Sugai, Genes Cells **9**, 765 (2004).
[52] J. E. Cabrera and D. J. Jin, Mol. Microbiol. **50**, 1493 (2003).
[53] J. E. Cabrera and D. J. Jin, J. Bacteriol. **188**, 4007 (2006).
[54] S. S. Andrews and A. P. Arkin, Biophys. J. BioFAST 106.102343 (2007).
[55] A. J. Levine, T. B. Liverpool, and F. C. MacKintosh, Phys. Rev. Lett. **93**, 038102 (2004).
[56] G. van der Heijden and J. Thompson, Nonlinear Dyn. **21**, 71 (2000).
[57] X. Yao, M. Jericho, D. Pink, and T. Beveridge, J. Bacteriol. **181**, 6865 (1999).
[58] J. Howard, *Mechanics of Motor Proteins and the Cytoskeleton* (Sinauer Associates, Sunderland, MA, 2001).
[59] A. Mogilner and G. Oster, Biophys. J. **84**, 1591 (2003).
[60] X. Liu and G. H. Pollack, Biophys. J. **83**, 2705 (2002).
[61] K. Luby-Phelps, D. Taylor, and F. Lanni, J. Cell Biol. **102**, 2015 (1986).